Journal of Organometallic Chemistry, 382 (1990) 129–141
Elsevier Sequoia S.A., Lausanne – Printed in The Netherlands
JOM 20561

Transition metal complexes of diazenes.

XXVI * Electrochemical study on group VIb dimetallaheterocycles: CO-substitution by electron transfer catalysis **

Peter Holzmeier, Horst Kisch *,

Institut für Anorganische Chemie der Universität Erlangen-Nürnberg, Egerlandstrasse 1, D-8520 Erlangen (F.R.G.)

and Jay K. Kochi

Department of Chemistry, University of Houston, University Park, Houston, Texas 77204 (U.S.A.)

(Received July 3rd, 1989)

Abstract

The electrochemistry of the dimetallacycles $(CO)_4M(\mu\text{-PMD})_2M(CO)_4$ (**1**) (M = Cr, Mo, W; PMD = pentamethylenediazirine) was studied at a Pt electrode in dichloromethane. All three compounds exhibit reversible one-electron oxidation as well as reduction, whereas the reduction to the dianions is irreversible on the CV time scale. Generation of the anion radicals in the presence of added phosphine (PEt_3) entails efficient ligand substitution following an electron transfer chain (ETC) mechanism. The reaction yields the mono- and the di-substitution products $(CO)_4M(\mu\text{-PMD})_2M(CO)_3PEt_3$ (**2**) and $Et_3P(CO)_3M(\mu\text{-PMD})_2M(CO)_3PEt_3$ (**3**), respectively. In the case of molybdenum and tungsten the single bridged complex $Et_3P(CO)_4M(\mu\text{-PMD})M(CO)_4PEt_3$ (**4**), formed via elimination of one diazirine ligand, is obtained as a by-product. Adjustment of the applied cathodic potential allows either substitution of one or two carbonyl ligands to be carried out selectively.

Introduction

In organometallic chemistry there has been an increasing interest in reactions involving intermediates with an odd number of valence electrons since the first

* For part XXV see ref. 1.
** Dedicated to Prof. Dr. G. Wilke on the occasion of his 65th birthday.

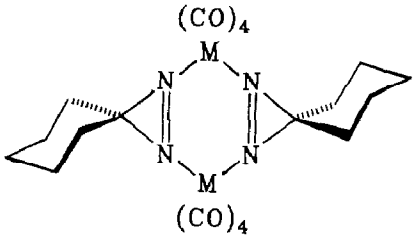

1a M = Cr
1b M = Mo
1c M = W

electrode-catalyzed reaction was reported by Elving et al. [2] in 1959. Among the different types of reactions that can be initiated by one-electron transfer the redox-induced ligand substitution in organometallic carbonyl complexes has gained by far the widest distribution. Starting from a neutral 18-electron metal carbonyl compound the transient intermediate in a redox-catalyzed chain process can be either a 17-electron radical cation or a 19-electron radical anion. This type of oxidation- or reduction-induced reaction is now usually referred to as electron-transfer chain (ETC) catalysis [3]. There are numerous examples of mono- and bi-nuclear carbonyl complexes which undergo ETC catalyzed substitution reactions via a 17-electron intermediate [3,5–8]. In contrast, the reductive ETC mechanism is largely restricted to polynuclear cluster compounds [3,9–12]; for mononuclear carbonyl complexes or dinuclear compounds lacking a metal–metal bond reduction-induced ligand substitution is known only in a few cases [13–15].

We have recently reported on the substitution photochemistry of the diazene dimetallacycles $M_2(PMD)_2(CO)_8$ (PMD = pentamethylenediazirine) (**1**) [1]. In the present study we examined the compounds **1a**–**1c** (M = Cr, Mo, W) by transient and bulk electrochemical techniques in order to compare their redox-induced reactivity with their photochemical behaviour. In this connection we have focussed our attention on the substitution chemistry of the electrochemically generated radical anions.

Results and discussion

The oxidation and reduction peak potentials of the three dimetallacycles $M_2(PMD)_2(CO)_8$ (**1**) (M = Cr, Mo, W), obtained from cyclic voltammetry in dichloromethane solution at room temperature, are given in Table 1. The cyclic voltammograms of the chromium and the molybdenum complex (**1a** and **1b**) are depicted in Fig. 1; the cathodic scan voltammogram of the tungsten complex **1c** is very similar to that of **1b**.

Each of the three complexes shows two successive reduction waves upon an initial negative-potential scan. On the reverse positive scan significant differences are observed, however. Whereas **1a** exhibits a completely irreversible behaviour for both reduction waves C_1 and C_2 (Fig. 1a), an anodic peak A_1 appears for **1b** (Fig. 1b) and **1c**. If the negative scan is reversed after the first reduction wave C_1, the

Table 1

Voltammetric peak potentials of the dimetallacycles 1 [a]

	Reduction			Oxidation	
	E_p^c	E_p^a	E_p^c	E_p^a	E_p^c
1a	−1.64	–	−1.98	0.75	0.58
1b	−1.26	−1.14	−1.70	0.95	0.81
1c	−1.11	−0.98	−1.63	0.91	–

[a] V vs. SCE; 2×10^{-3} *M* in dichloromethane containing 0.1 *M* $TBAPF_6$; sweep rate 0.5 V/s.

peak current of A_1 is increased relative to that of C_1 (e.g. the i_p^a/i_p^c ratio is raised from 0.4 to 0.8 for **1b**) (Fig. 1b). As can be judged from calibration of the cathodic peak current of C_1 with a ferrocene standard [16], these two peaks constitute an

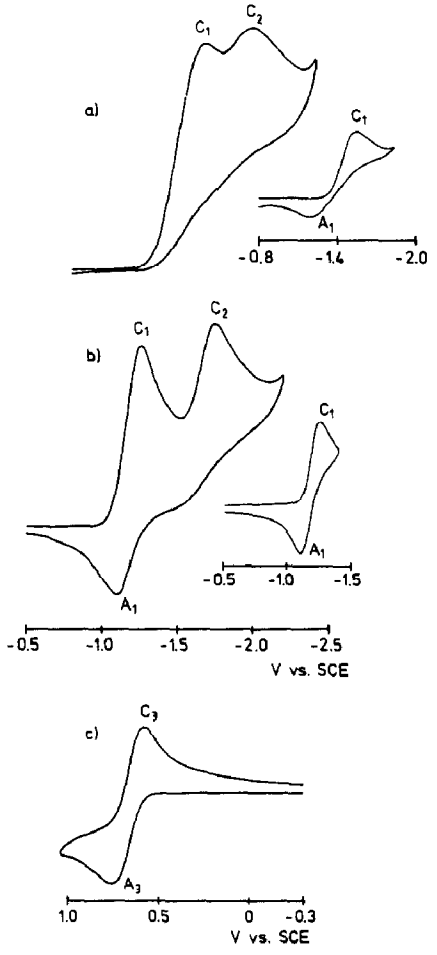

Fig. 1. Cyclic voltammograms of the dimetallacycles **1** (2×10^{-3} *M* in dichloromethane containing 0.1 *M* $TBAPF_6$; sweep rate 0.5 V/s). (a) initial cathodic scan voltammogram of **1a**; inset shows quasi-reversible behaviour of the first reduction wave C_1 at −21°C. (b) **1b** (initial cathodic scan); inset illustrates reversibility of C_1. (c) **1a** (initial anodic scan).

electrochemically reversible one-electron redox couple (ΔE_p 63 mV [17*]); sweep rate 0.5 V/s). For **1a** an anodic peak A_1 can only be observed at low temperatures (−20 °C to −40 °C) (Fig. 1a); the redox couple then becomes quasi-reversible ($\Delta E_p = 190$ mV [17*]; sweep rate 0.5 V/s). The same effect can be achieved by raising the sweep rate to values above 200 V/s. Thus, it can be concluded that in the case of the chromium complex **1a** the anion radical is much more reactive than in the case of molybdenum (**1b**) and tungsten (**1c**). The absence of the reverse electron-transfer step at room temperature for **1a** and the ratio of anodic and cathodic peak currents of below unity for **1b** and **1c** is likely to derive from rapid dissociative decomposition of the anion radicals (eq. 1).

$$M_2(PMD)_2(CO)_8^{\cdot -} \rightarrow M_2(PMD)_2(CO)_7^{\cdot -} + CO \quad (1)$$

This assumption gets further support from the fact that in the case of **1b** the ratio of anodic and cathodic peak currents for the first reduction step is significantly increased in CO-saturated solution (i.e. $i_p^a/i_p^c = 1.0$ under CO but only 0.8 under N_2). A similar effect of CO could be observed for the one-electron reduction of several triiron carbonyl clusters [12]. For all three complexes a high lability also applies for the dianion since the second reduction step C_2 remains irreversible even at low temperatures or higher scan rates. In the series $M(CO)_4$bpy (M = Cr, Mo, W) [13] the potential of the chromium complex **1a** is more negative by 0.4 V as compared to the molybdenum and the tungsten complex.

On the oxidative branch of the cyclic voltammogram each of the three complexes shows an anodic wave A_3 that can be attributed to a one-electron oxidation by calibration with ferrocene [16]. The associated reduction peak C_3 can only be observed for **1a** (Fig. 1c) and **1b**, whereas the oxidation of **1c** is irreversible at room temperature. The i_p^c/i_p^a values for **1a** and **1b** are 0.9 and 0.1, respectively, showing an increasing share of decomposition of the cation radical in the order Cr < Mo < W. Especially when anodic scans are performed, the shape and position of the peaks for each of the three complexes is critically dependent on the treatment of the Pt electrode surface. Only by careful cleaning can well-defined voltammograms be obtained. Running a few scans in succession causes the peaks to broaden and decrease in intensity, which indicates coating of the electrode by decomposition products.

These results show that the dimetallacycles **1** can be subjected to one-electron oxidation as well as one- and two-electron reduction. Whereas the formation of the dianion proves to be chemically irreversible on the CV time scale, partial chemical reversibility is observed for the anion and cation radicals. This points to the possibility of a redox-induced substitution chemistry.

In order to get some insight into the chemical reactivity of the electrogenerated odd-electron species we examined the transient electrochemical behaviour of the complexes **1** in the presence of added phosphine and phosphite ligands. Knowing the results of Miholová and Vlček [13] upon the reduction-induced substitution chemistry of the tetracarbonyl complexes $M(CO)_4$bpy (M = Cr, Mo, W; bpy = 2,2′-bipyridine) which are comparable to our complexes with respect to the coordination sphere around their central metals, we focussed our attention on the reactivity of the

* Reference number with asterisk indicates a note in the list of references.

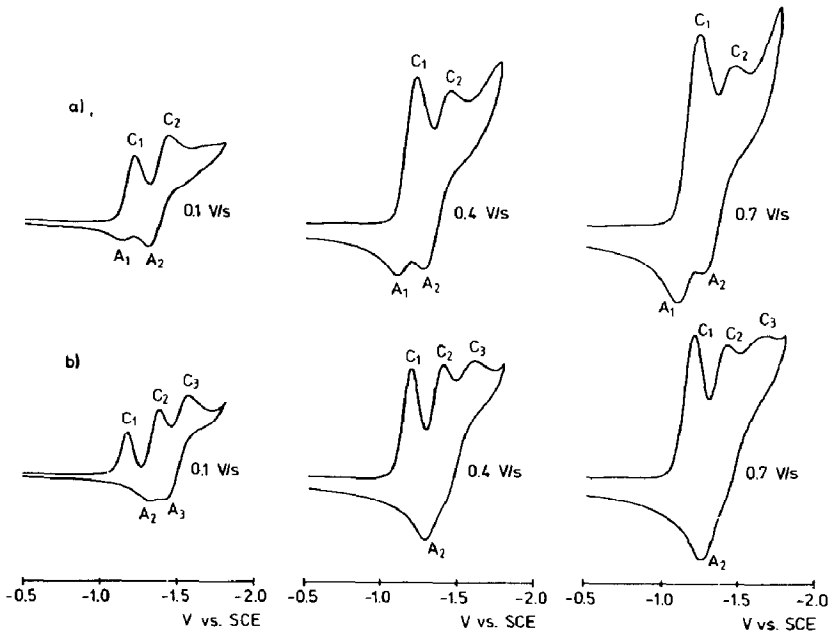

Fig. 2. (Row a) Cyclic voltammograms obtained on the initial cathodic scan of a 2×10^{-3} *M* dichloromethane solution of **1b** containing 4×10^{-3} *M* PEt_3 and 0.1 *M* $TBAPF_6$ at increasing sweep rates. (Row b) The cyclic voltammograms of the same solution but containing 10^{-2} *M* PEt_3.

anion radicals. Beyond this, we did not notice any observable impact of an excess of added phosphine ligand (PPh_3 and PEt_3) on the shape of the cyclic voltammogram for any of the three complexes **1** upon an initial anodic scan.

On the contrary, a distinct alteration in the initial cathodic scan voltammogram of the molybdenum complex **1b** can be observed in the presence of several phosphorus ligands. Thus, Fig. 2 shows cyclic voltammograms of a solution of **1b** containing various concentrations of PEt_3 taken at different sweep rates.

In particular the presence of a twofold excess of triethylphosphine gives rise to a new reduction peak C_2 (E_p^c −1.46 V vs. SCE; sweep rate 0.4 V/s) and its anodic counterpart A_2 (E_p^a −1.28 V) (Fig. 2a). From a comparison with the cyclic voltammogram of an authentic sample this peak couple can be attributed to the monosubstitution product $Mo_2(PMD)_2(CO)_7PEt_3$ (**2b**). A decrease of the peak currents of C_2 and A_2 relative to those of the reactant waves C_1 and A_1 can be achieved by increasing the CV sweep rate. This behaviour is in agreement with the assumption that **2b** is formed by the reaction of the anion radical of **1b** with PEt_3 via ligand substitution. Raising the concentration of phosphine to a 5-fold excess leads to the cyclic voltammograms depicted in Fig. 2b. Two features in this figure are noteworthy. First, in addition to the reduction wave C_2 attached to **2b** a third cathodic peak C_3 (−1.62 V vs. SCE; sweep rate 0.4 V/s) appears. At slow sweep rates ($\leq$ 0.1 V/s) the associated anodic peak A_3 can also be observed. A comparison of the peak potentials of C_3 and A_3 with those of an authentic sample reveals their relationship to the disubstitution product $Mo_2(PMD)_2(CO)_6(PEt_3)_2$ (**3b**). The second feature to be noticed is the complete disappearance of the anodic peak A_1 related to **1b**. This requires that the anion radical of **1b** is removed from the vicinity of the electrode by some chemical reaction before its oxidation potential is reached

on the reverse positive scan. This reaction is the formation of the monosubstitution product **2b** which is clearly in evidence by the appearance of its CV waves C_2 and A_2. Subsequently the disubstitution product **3b** is formed. The bulk electrolysis experiments described in the following section will show that this second substitution reaction is following the same mechanism as the first one, i.e. electron-transfer induced chain catalysis.

Detailed studies of the heterogeneous electrode kinetics of ETC catalytic processes [5,20,21] have revealed that the general mechanism of these electrocatalytic processes consists of an initiation step (eq. 2):

$$M_x(CO)_n + e^- \rightarrow M_x(CO)_n^{\cdot -} \tag{2}$$

followed by the substitution reaction (eq. 3):

$$M_x(CO)_n^{\cdot -} + L \rightarrow M_x(CO)_{n-1}L^{\cdot -} + CO \tag{3}$$

and the cross redox-reaction (eq. 4) being the most vital point in the overall mechanism:

$$M_x(CO)_{n-1}L^{\cdot -} + M_x(CO)_n \rightarrow M_x(CO)_{n-1}L + M_x(CO)_n^{\cdot -} \tag{4}$$

The crucial requirement about the redox potentials (E^0) of the starting material (MCO) and the substituted compound (ML) for a reduction-induced cycle to proceed is $E^0_{ML} < E^0_{MCO}$. As can be seen from the cyclic voltammograms in Fig. 2 this condition is fulfilled in the present case. For the reduction-induced ligand substitution in several triiron clusters [12] it could be shown that the substitution reaction in eq. 3 is likely to follow a dissociative rather than an associative mechanism. Although the enhancement of the ratio i^a_p/i^c_p for the first reduction step of the molybdenum complex **1b** caused by addition of carbon monoxide points to a dissociative mechanism, the reaction rate is shown to be dependent on the nature of the added phosphorus ligand. This is exemplified by Fig. 3 where cyclic voltammograms of a solution of **1b** containing a twofold excess of trimethylphosphite (a) and triethylphosphine (b) are displayed.

Both voltammograms consist of the reactant waves C_1 and A_1 and the peak couple C_2 and A_2 arising from the transient formation of the monosubstitution product. The marked difference between the relative peak currents of the reduction waves C_2 in both cases suggests a direct correlation between the nucleophilicity of the phosphorus ligand and the rate of the substitution reaction. These findings lead to the assumption of a partly associative character of the CO substitution in the radical anion of **1b**. However, without further kinetic studies a more detailed discussion of the reaction mechanism cannot be given at the present time.

Addition of a phosphine ligand also leads to significant alterations in the transient chemical behaviour of the chromium complex **1a**. This situation is displayed in Fig. 4.

As already shown, the cyclic voltammogram of **1a** consists of two irreversible reduction waves C_1 and C_2 (Fig. 4a). However, when 0.25 equivalents of triethylphosphine are added to the solution a considerable decrease of the first reactant wave C_1 can be observed. Simultaneously a new irreversible cathodic peak C_3 (E^c_p -1.77 V vs. SCE; sweep rate 0.1 V/s) appears (Fig. 4b) which can be attributed to the substitution product $Cr_2(PMD)_2(CO)_7PEt_3$ (**2a**) by comparison with an authentic sample. When the concentration of PEt_3 is increased to one equivalent, C_1 is diminished to a small remainder and besides a further increase of C_3 the

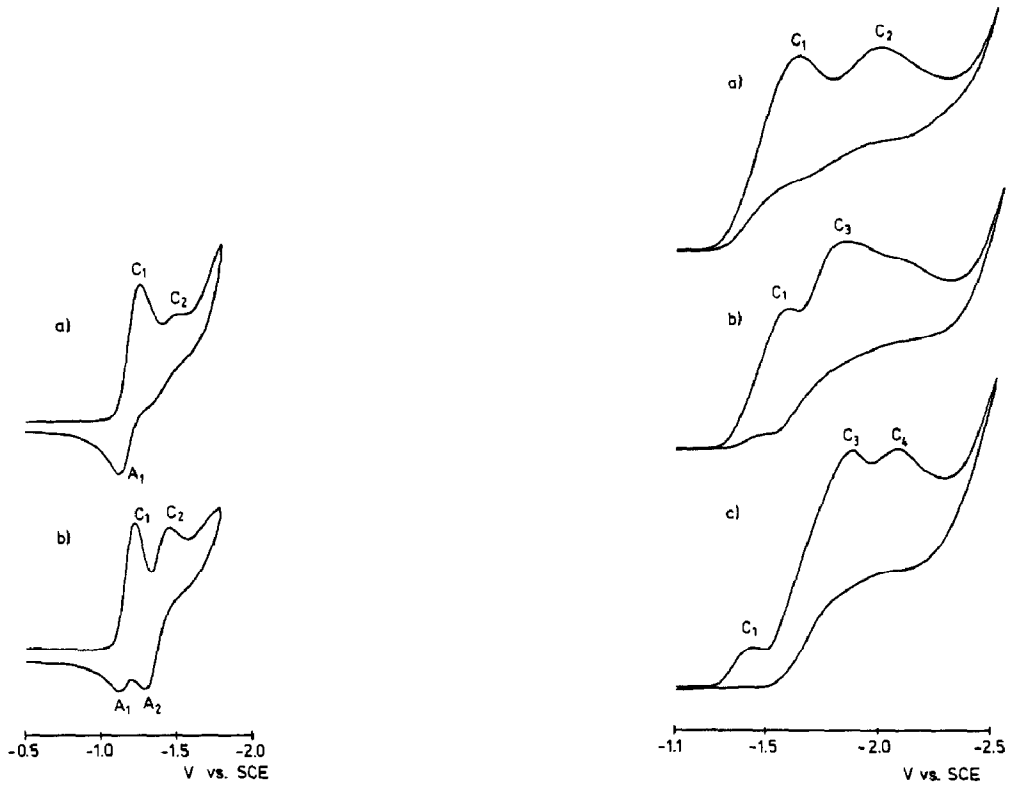

Fig. 3. Initial cathodic scan voltammograms of a 2×10^{-3} *M* dichloromethane solution of **1b** (0.1 *M* $TBAPF_6$) containing 4×10^{-3} *M* $P(OMe)_3$ (a) and 4×10^{-3} *M* PEt_3 (b); sweep rate 0.4 V/s.

Fig. 4. (a) Cyclic voltammogram (initial cathodic scan) of a 5×10^{-3} *M* dichloromethane solution of **1a** containing 0.1 *M* $TBAPF_6$ (sweep rate 0.1 V/s). (b) Cyclic voltammogram of the same solution as in (a) but containing 1.3×10^{-3} *M* PEt_3. (c): 5×10^{-3} *M* PEt_3.

reduction wave C_4 (E_p^c −1.97 V) of the disubstitution product $Cr_2(PMD)_2(CO)_6(PEt_3)_2$ (**3a**) can be observed (Fig. 4c). As in the case of the molybdenum complex **1b** it can be concluded that the phenomenon shown in Fig. 4 is associated with rapid interception of the electrochemically generated anion radical of the dimetallacycle by the phosphine ligand.

In contrast to the behaviour of **1a** and **1b** the initial cathodic scan voltammogram of the tungsten dimetallacycle **1c** appears to be unaffected by the presence of added phosphorus ligands. In no case could a CV wave corresponding to the mono- or di-substitution product be observed. We therefore concentrated our interest on **1a** and **1b**, although bulk electrolysis experiments reveal that redox-induced substitution reactions can also be performed with **1c**.

Substitution of CO with several phosphine ligands L (L = PPh_3, PEt_3, dppe) in the chromium complex **1a** has recently been carried out photochemically (eq. 5) [1].

$$\underset{(1)}{M_2(PMD)_2(CO)_8} + L \xrightarrow{h\nu} \underset{(2)}{M_2(PMD)_2(CO)_7L} + CO \qquad (5)$$

Continued irradiation in the presence of a 5-fold excess of triethylphosphine entails

the substitution of a second CO ligand (eq. 6) [18].

$$\mathbf{2} + L \xrightarrow{h\nu} \underset{(\mathbf{3})}{M_2(PMD)_2(CO)_6L_2} + CO \qquad (6)$$

As indicated by the electrocatalytic behaviour of the cyclic voltammograms of **1a** and **1b** efficient substitution of one or two CO ligands in the dimetallacycles **1** can be carried out selectively by electrostimulation at controlled negative potentials. Thus, inserting a set of platinum electrodes into a dichloromethane solution of **1b** containing an excess of triethylphosphine and applying a negative potential of −1.15 V (vs. SCE) leads to the formation of the monosubstitution product $Mo_2(PMD)_2(CO)_7PEt_3$ (**2b**). Coulometry during this bulk electrolysis experiment, carried out at constant potential, reveals an efficient ETC catalysis. From the measurement of the amount of charge passed through the solution a current efficiency of 68 equivalents of **1b** is obtained per electron. The disubstitution product $Mo_2(PMD)_2(CO)_6(PEt_3)_2$ (**3b**) is obtained when the electrolysis is continued at a potential of −1.29 V. The current efficiency for the substitution of the second CO ligand was found to be 37 equivalents per electron. The end of both electrolysis steps can conveniently be determined by monitoring the concentrations of **1b** and **2b**, respectively, by cyclic voltammetry. An additional indication is given by the cathodic current of the potentiostatic experiment which is relatively constant at ≈ 5 mA for approximately 1–2 min and then abruptly decreases to zero. Both substitution steps are also apparent by significant changes in the UV-VIS spectrum, since substitution of CO by better σ-donor ligands like phosphine in the dimetallacycles **1** causes a distinct bathochromic shift of their CTML absorption which lies in the range of 460–480 nm. Figure 5 shows these UV-VIS spectra changes for the substitution products of **1b**.

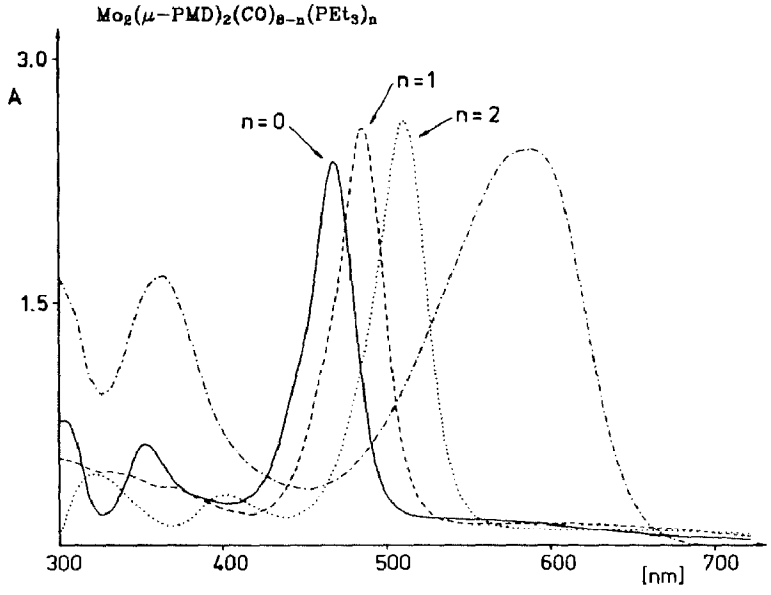

Fig. 5. UV-VIS absorption spectra of **1b** (———), **2b** (— — —), **3b** (· · · · · ·) and **4b** (· — · — ·) in toluene.

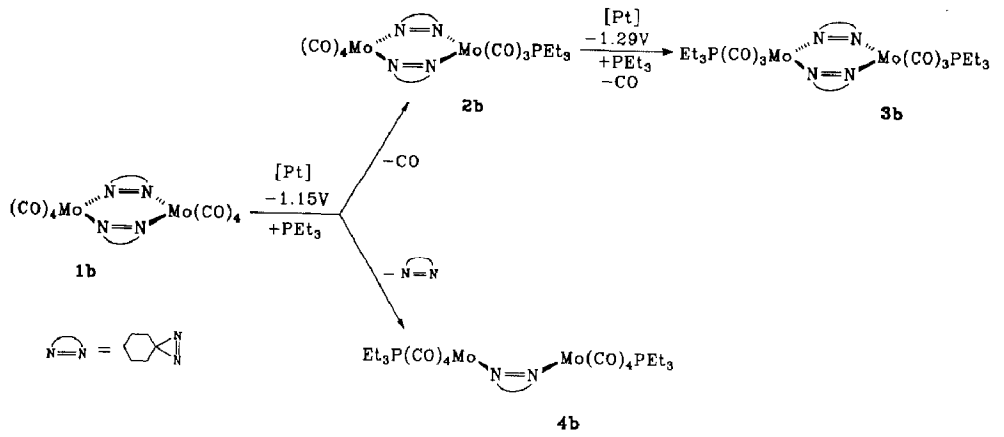

Fig. 6. Proposed reaction scheme for the reduction -induced ligand substitution of **1b**.

The close similarity of the IR spectra of the disubstitution product **3b**, obtained by electrochemical reduction and the photochemically synthesized complex $Cr_2(PMD)_2(dppe)(CO)_6$ [1], where dppe acts as a bridging ligand, reveals that the two PEt_3 ligands in **3b** are coordinated at two different metal centers. This seems plausible since an increase in electron density at one molybdenum atom, caused by introduction of a phosphine ligand after the first substitution step, is likely to impede further reduction at the same metal center.

Besides CO-substitution leading to the dimetallacycles **2b** and **3b** a second reaction pathway can be observed during the electrochemical reduction of **1b** in the presence of triethylphosphine. Chromatographic work-up of the catholyte after the first electrolysis step at −1.15 V yields **2b** and additionally a deep blue compound that could be identified as $PEt_3(CO)_4Mo(PMD)Mo(CO)_4PEt_3$ (**4b**) (Fig. 6). The UV-VIS spectrum of this single bridged complex like those of the dimetallacycles **1** to **3** exhibits the typical pattern of the chromophor M(RN=NR)M [19]; however, in comparison to the dimetallacycles its CTML absorption at 589 nm (toluene) is significantly broadened and shifted to lower energy (Fig. 5). These findings are in good agreement with the spectroscopic properties of the unsubstituted single bridged compounds $(CO)_5M(PMD)M(CO)_5$ (M = Cr, Mo, W) [19].

An analogous by-product **4c** could be observed during the electrolysis of the tungsten complex **1c**. The appearance of **4b** after the first electrostimulated substitution step of **1b** (i.e. at a cathodic potential where the starting material but not the monosubstitution product **2b** is reduced) excludes its formation via the anion radical of **2b**; since a solution of **2b** containing an excess of PEt_3 ramains unchanged for several hours, its formation via thermal reaction of **2b** can also be excluded. Therefore we propose that **4b** arises from M–N bond cleavage and subsequent phosphine coordination in the anion radical derived from **1b**. It can be concluded that an increase in electron density in the dimetallacycle caused by electrochemical reduction weakens both the metal–CO and the metal–diazirine bonds. This results in two different reaction pathways as shown in Fig. 6. A comparable effect, destabilization and cleavage of the M–N bonds, caused by introduction of strong σ-donors like amine ligands could be observed for **1a** [1].

Bulk electrolysis experiments carried out under reduction conditions with the chromium and the tungsten dimetallacycle (**1a** and **1c**, respectively) in the presence of triethylphosphine also reveal ETC catalyzed ligand substitution. For the first electrolysis step of **1a** and **1c** the current efficiencies are 9 and 14 equivalents per electron, respectively. Thus, the efficiency of the electrocatalytic cycle is highly dependent on the metal, decreasing in the order Mo $\gg$ W > Cr. A similar sequence was found by Hershberger et al. [22] for the oxidation-induced ligand substitution of several mononuclear Group VIb complexes. Whereas in the case of **1c** the reaction follows the same scheme as proposed for **1b** (i.e. CO substitution and cleavage of the dimetallacycle, see Fig. 6), **1a** solely yields the mono- and di-substituted dimetallacycles $Cr_2(PMD)_2(CO)_7PEt_3$ (**2a**) and $Cr_2(PMD)_2(CO)_6(PEt_3)_2$ (**3a**), indicating a higher stability of the metal–diazirine bonds in the chromium complex.

The results obtained in this study offer a good example of the high selectivity that can be achieved in electron-transfer induced ligand substitution. Whereas both thermal and photochemical reactions of the dimetallacycles **1** with strong ligands like triethylphosphine yield a mixture of mono- and di-substitution products, the degree of substitution in the electrochemical reaction can be controlled by adjustment of the applied potential.

Experimental

Materials. All manipulations with metal carbonyls were carried out under a nitrogen atmosphere. Dichloromethane used for electrochemistry was vigorously stirred with sulfuric acid for 24 h, then washed neutral with an aqueous solution of $NaHCO_3$ and dried over $CaCl_2$. This was followed by distillation from P_2O_5 and subsequently from CaH_2. To minimize the residual water content the solvent was finally passed through a column containing freshly activated alumina (Woelm). Hydrocarbon solvents where freshly distilled from sodium. Silica gel (Merck, 230–400 mesh) for chromatography was degassed and kept under nitrogen. The complexes **1** were prepared and purified according to the literature [19]. The ligands triethylphosphine and trimethylphosphite (Aldrich) were stirred over sodium for several hours and then distilled from CaH_2. Tetra-n-butylammoniumhexafluorophosphate ($TBAPF_6$) (Aldrich) which was used as supporting electrolyte was recrystallized from ethyl acetate and dried in vacuo at 130 °C.

Instrumentation. Infrared spectra were recorded with a Perkin Elmer 983, UV-VIS spectra with a Shimadzu 260 spectrophotometer. Most of the cyclic voltammograms were measured in Houston, using a set-up as described elsewhere [23]. Additional measurements in Erlangen were performed with a Wenking PGS 77 potentiostat driven by a Wenking VGS 72 voltage scan generator. The CV cell used in both cases was of air-tight design equipped with high-vacuum Teflon valves for maintainance of an inert atmosphere. The platinum-disk working electrode, embedded in a glass seal, was periodically polished. All given potentials are referenced to SCE which was separated from the working-electrode compartment by a sintered glass frit. The counter electrode consisted of a platinum gauze that was separated from the working electrode by $\approx$ 3 mm.

Bulk electrolysis was carried out either with a Princeton Applied Research (PAR) Model 173 potentiostat/galvanostat equipped with a PAR Model 179 digital coulometer or with a Wenking PGS 77 potentiostat/galvanostat. The three-cham-

bered electrochemical cell was of air-tight design and allowed a CV working electrode to be inserted. Thus, the electrochemical reaction could conveniently be monitored. A platinum plate with a surface of ≈ 3 cm^2 was used as working electrode. All electroreductions were carried out at constant potential. The reaction was followed by periodical measurement of a cyclic voltammogram or UV-VIS spectroscopy and TLC of an aliquot extracted from the catholyte.

*Heptacarbonylbis(pentamethylenediazirine)triethylphosphinedimolybdenum(0) (**2b**)*

The electrolysis cell was charged with a dichloromethane solution of 0.13 g (0.20 mmol) of **1b** and 0.12 g (1.0 mmol) of PEt_3 containing 0.1 *M* $TBAPF_6$ as supporting electrolyte. A cathodic current at a constant potential of -1.15 V was passed through the solution. The reaction showed to be completed by rapid decrease of the initial current of ≈ 5 mA to zero after 90 s. At this time the first cathodic wave C_1 of **1b** (Fig. 1b) was absent in the cyclic voltammogram. For the removal of the supporting electrolyte the reaction mixture was evaporated to dryness, the residue redissolved in toluene and filtered. Chromatography of the filtrate with n-hexane/dichloromethane (3/1) gave first a very small greenish yellow band of unreacted **1b**. With increasing ratio of dichloromethane/n-hexane a deep blue fraction and subsequently the major greenish brown band of **2b** were eluted. This latter fraction was concentrated in vacuo to ≈ 5 ml. Addition of 40 ml of n-hexane precipitated dark green microcrystals of **2b**. After cooling to $-20\,^\circ$C for several hours to complete the precipitation they were collected by filtration; 79 mg (53% yield).

Found: C, 41.73; H, 4.97; N, 7.36. $C_{25}H_{35}Mo_2N_4O_7P$ (726.43) calcd.: C, 41.34; H, 4.86; N, 7.71%. IR (ν(CO) cm^{-1}, toluene): 2026 m, 1954 vs, 1926 s, 1898 m, 1882 s, 1868 sh. UV-VIS (nm, toluene) ($\epsilon \times 10^3$): 486 (50.3), 370 (7.13), 336 (8.71).

The deep blue fraction was identified as complex **4b** (Fig. 6) by mass spectroscopy and by comparison of its UV-VIS and IR data with those of $(CO)_4Cr(PMD)(dppm)Cr(CO)_4$ (dppm = $Ph_2PCH_2PPh_2$), the structure of which was established by X-ray analysis [24].

IR (ν(CO), cm^{-1}, toluene): 2012 vs, 2004 m, 1909 vs, 1894 vs, 1875 vs.

*Hexacarbonylbis(pentamethylenediazirine)bis(triethylphosphine)dimolybdenum(0) (**3b**)*

After the first electrolysis step described above the potential was set to -1.29 V. The reaction was completed within 2 min as indicated by the disappearance of the first cathodic CV wave of **2b** (C_2 in Fig. 2). Chromatographic work-up as above yielded 78 mg (47%) of dark green crystals.

Found: C, 43.42; H, 6.06; N, 6.48. $C_{30}H_{50}Mo_2N_4O_6P_2$ (816.58) calcd.: C, 44.13; H, 6.17; N, 6.86% IR (ν(CO), cm^{-1}, toluene): 1970 s, 1920 vs, 1887 sh, 1878 s, 1852 s. UV-VIS (nm, toluene) ($\epsilon \times 10^3$): 511 (72.0), 303 (8.64), 321 (14.2).

*Heptacarbonylbis(pentamethylenediazirine)triethylphosphinedichromium(0) (**2a**)*

A dichloromethane solution of 0.11 g (0.20 mmol) of **1a** and 0.12 g (1.0 mmol) of PEt_3 containing 0.1 *M* $TBAPF_6$ was electrolyzed at a constant potential of -1.38 V. The reaction was completed after 10 min as indicated by the decrease of the initial current of ≈ 5 mA to zero. Chromatographic work-up as above besides a small amount of the disubstitution product **3a** yielded dark blue crystals of **2a**; 94 mg (73% yield).

Found: C, 46.81; H, 5.83; N, 8.24. $C_{25}H_{35}Cr_2N_4O_7P$ (638.55) calcd.: C, 47.03; H, 5.52; N, 8.77%. IR (ν(CO), cm^{-1}, toluene): 2020 m, 1946 s, 1925 vs, 1899 m, 1881 s, 1863 m. UV-VIS (nm, toluene) ($\epsilon \times 10^3$): 501 (38.2), 365 (10.9), 335 (9.45).

*Hexacarbonylbis(pentamethylenediazirine)bis(triethylphosphine)dichromium(0) (**3a**)*

After the first reduction step described above the electrolysis was continued at a constant potential of -1.51 V until the initial current of ≈ 5 mA decreased to zero. Chromatographic work-up as above yielded 95 mg (65%) of dark green crystals).

Found: C, 49.10; H, 7.55; N, 7.01. $C_{30}H_{50}Cr_2N_4O_6P_2$ (728.70) calcd.: C, 49.45; H, 6.92; N, 7.69%. IR (ν(CO), cm^{-1}, toluene): 1962 s, 1910 vs, 1893 m, 1876 s, 1849 vs. UV-VIS (nm, toluene) ($\epsilon \times 10^3$): 534 (26.1), 423 (6.18), 359 (6.97).

*Bulk electrolysis of **1c** in the presence of triethylphosphine*

A dichloromethane solution of 0.10 g (0.12 mmol) of **1c** and 0.07 g (0.6 mmol) of PEt_3 containing 0.1 *M* $TBAPF_6$ was electrolyzed in two steps at constant potentials of -1.10 and -1.35 V. After the second reduction step, the completion of which was indicated by the decrease of the initial current of ≈ 4 mA to zero, the catholyte was worked up as above yielding a deep blue and a reddish violet fraction. The latter could be identified as $W_2(PMD)_2(CO)_6(PEt_3)_2$ (**3c**) by mass spectroscopy and by its UV-VIS and IR data.

IR (ν(CO), cm^{-1}, toluene): 1967 s, 1912 vs, 1888 sh, 1873 s, 1846 vs. UV-VIS (nm, toluene): 517, 393, 321.

For the deep blue compound IR and mass spectroscopic data as well as its UV-VIS pattern with a broad absorption band at 626 nm suggest the same structure as for the single bridged complex **4b**: $W_2(PMD)(CO)_8(PEt_3)_2$ (**4c**).

IR (ν(CO), cm^{-1}, toluene): 1994 vs, 1920 sh, 1905 vs, 1888s.

Acknowledgement

We wish to thank T.M. Bockman for helpful discussions. This work was financially supported by Stiftung Volkswagenwerk and Fonds der Chemischen Industrie.

References

1 Part XXV: P. Holzmeier, H. Görner, F. Knoch, H. Kisch, Chem. Ber., 122 (1989) 1457.
2 P.J. Elving, B. Zemel, Can. J. Chem., 17 (1959) 247.
3 J.K. Kochi, J. Organomet. Chem., 300 (1986) 139, and ref. therein.
4 For a general discussion of the ETC mechanism see: M. Chanon, M.L. Tobe, Angew. Chem., 94 (1982) 27; Angew. Chem. Internat. Edit., 21 (1982) 1.
5 J.W. Hershberger, C. Amatore, J.K. Kochi, J. Organomet. Chem., 250 (1983) 345.
6 For a review see: N.G. Connelly, W.E. Geiger, Adv. Organomet. Chem., 23 (1984) 1; D. Astruc, Angew. Chem., 100 (1988) 662.
7 M.E. Khalifa, M. Gueguen, R. Mercier, F.Y. Petillon, J.Y. Saillard, J. Talarmin, Organometallics, 8 (1989) 140.
8 G.J. Bezems, P.H. Rieger, S. Visco, J. Chem. Soc. Chem. Comm., (1981) 265.
9 S. Jensen, B.H. Robinson, J. Simpson, J. Chem. Soc. Chem. Comm., (1983) 1081.
10 P. Lahuerta, J. Latorre, M. Sanau, H. Kisch, J. Organomet. Chem., 286 (1985) C27.
11 M.G. Richmond, J.K. Kochi, Inorg. Chem., 25 (1986) 656; H.H. Ohst, J.K. Kochi, ibid., 25 (1986) 2066; J. Am. Chem. Soc., 108 (1986) 2897.

12 T.M. Bockman, J.K. Kochi, J. Am. Chem. Soc., 109 (1987) 7725.
13 D. Miholová, A.A. Vlček, J. Organomet. Chem., 240 (1982) 413; 279 (1985) 317.
14 F.R. Estevan, P. Lahuerta, J. Latorre, Inorg. Chim. Acta, 116 (1986) L33.
15 B. Olbrich-Deussner, W. Kaim, J. Organomet. Chem., 340 (1988) 71; 361 (1989) 335.
16 R.R. Gagne, C.A. Koval, G.C. Lisensky, Inorg. Chem., 19 (1980) 2854.
17 The ΔE_p values were calibrated by linear correction relative to a ferrocene standard under identical experimental conditions [16].
18 P. Holzmeier, H. Kisch, unpublished results.
19 R. Battaglia, H. Matthäus, H. Kisch, J. Organomet. Chem., 193 (1980) 57.
20 D. Garreau, J.M. Saveant, J. Electroanal. Chem., 35 (1972) 309; 50 (1974) 1.
21 J.W. Hershberger, R.J. Klinger, J.K. Kochi, J. Am. Chem. Soc., 105 (1983) 61; P.M. Zizelman, C. Amatore, J.K. Kochi, ibid., 106 (1984) 3771.
22 J.W. Hershberger, R.J. Klinger, J.K. Kochi, J. Am. Chem. Soc., 104 (1982) 3034.
23 D.J. Kuchynka, C. Amatore, J.K. Kochi, Inorg. Chem., 25 (1986) 4087.
24 P. Holzmeier, F. Knoch, H. Kisch, unpublished results.